Supporting Information

Redox-coupled Quinone Dynamics in the Respiratory Complex I

Judith Warnau[a,b,†], Vivek Sharma[c,d,†,*], Ana P. Gamiz-Hernandez[a], Andrea Di Luca[a], Outi Haapanen[c], Ilpo Vattulainen[c,e,f], Mårten Wikström[d], Gerhard Hummer[b,*], Ville R. I. Kaila[a,*]

[a] Department Chemie, Technische Universität München, Lichtenbergstraße 4, D-85748 Garching, Germany.

[b] Department of Theoretical Biophysics, Max Planck Institute of Biophysics, Max-von-Laue-Straße 3, 60438 Frankfurt am Main, Germany.

[c] Department of Physics, University of Helsinki, PO Box 64, FI-00014, Helsinki, Finland.

[d] Institute of Biotechnology, University of Helsinki, FI-00014, Helsinki, Finland.

[e] Department of Physics, Tampere University of Technology, PO Box 692, FI-33101, Tampere, Finland.

[f] MEMPHYS – Center for Biomembrane Physics, Department of Physics, University of Southern Denmark, Odense, Denmark.

[†] Contributed equally to this work.

[*]E-mail: vivek.sharma@helsinki.fi; gerhard.hummer@biophys.mpg.de; ville.kaila@ch.tum.de

Table S1. Summary of simulation setups. 1) MD setup of complex I with Q_6 with 823,699 atoms; 2) MD setup of complex I with Q_{10} with 809,413 atoms; 3) MD setup of complex I with Q_6 or Q_1 with *ca*.180,000 atoms. His and Tyr refer to residues His-38 and Tyr-87 of subunit Nqo4. MD - unrestrained molecular dynamics simulations; US - umbrella sampling. See Methods section for details on Steered Molecular Dynamics (SMD) runs.

Active site	**Setup**	**Length**	**Type**
Q_{ox} $HisH^+$/TyrOH	1	350 ns	MD
	2	250 ns	MD
QH_2 His/$TyrO^-$	1	350 ns	MD
	2	250 ns	MD
QH_2 His/$TyrO^-$	1	5 x 6 ns	MD
Q_{ox} His/$TyrO^-$	1	175 ns	MD
QH_2 $HisH^+$/TyrOH	1	140 ns	MD
Q_{ox} $HisH^+$/TyrOH	3	61 x 15 ns	US
QH_2 His/$TyrO^-$	3	61 x 15 ns	US
Q_{ox} $HisH^+$/TyrOH	3	2 x 70 ns	MD*
QH_2 His/$TyrO^-$	3	2 x 70 ns	MD*
$Q_{ox}HisH^+$/TyrOH	2	65 x 11 ns	MD
QH_2 His/$TyrO^-$	2	57 x 11 ns	MD
Total simulation time:		4.997 μs	

* unbiased MD simulations with a Q_6 at site 2'.

Table S2. Analysis of ion-pairs dynamics (setup 2). Distance based on the ion-pair refined in the crystal structure (PDB ID: 4HEA), and ratio of closed and open ion-pairs when the Q_{ox} (red)/QH_2 (blue) headgroup resides in sites 1, 1', 2, 2'. The threshold for the ion-pair opening set to >5 Å.

	Crystal structure	**Ratio of closed/open ion-pairs for Q_{ox} and QH_2**							
Ion-pair	**Distance** [Å]	**Binding Site 1 (Q_{ox})**	**Binding Site 1' (Q_{ox})/ 1'(QH_2)**		**Binding Site 2,2' (Q_{ox})/2 (QH_2)**		**Binding Site 2,2'(Q_{ox})/2' (QH_2)**	
$Asp49_{Nqo7}/Lys146_{Nqo8}$	9.1	98/2	6/94	0/96	60/40	0/96	60/40	0/96
$Asp55_{Nqo6}/Arg62_{Nqo6}$	11.4	5/95	76/24	7/96	75/25	0/96	75/25	0/96
$Asp392_{Nqo4}/Arg21_{Nqo4}$	3.0	8/92	100/0	0/96	5/95	0/96	5/95	6/90
$Asp62_{Nqo8}/Arg36_{Nqo8}$	2.6	28/72	92/8	0/96	94/6	0/96	94/6	85/11
$Asp139_{Nqo4}/His38_{Nqo4}$	2.4	100/0	98/2	26/70	100/0	41/55	100/0	70/26
$Glu213_{Nqo8}/Arg294_{Nqo8}$	10.4	0/100	30/70	6/90	16/84	13/83	16/84	3/93
$Glu213_{Nqo8}/Arg216_{Nqo8}$	15.7	99/1	88/12	69/27	90/10	93/3	90/10	68/28

Table S3. List of conserved amino acids near the Q-channel in Nqo4, Nqo6, Nqo7-Nqo11. Conserved residues, amino acids essential for activity, and related to human diseases are marked in red (1-5). See also Fig. S8-S10 for sequence alignments of subunits that form the Q-tunnel of complex I (Nqo4, Nqo6 and Nqo8).

Nqo4	Nqo6	Nqo7	Nqo8	Nqo10	Nqo11
†Gln-33	†Trp-37	*Lys-40	‡Phe-28	*Tyr-59	*Glu-32
*His-34	Thr-40	*Glu-45	*Glu-35		Glu-67
*His-38	Gly-42	†Asp-49	*Arg-36		
*Gln-50	†Ala-47	†Tyr-62	*Gln-43		
*Arg-84	†Ile-48	*Asp-72	*Arg-45		
*Tyr-87	†Met-50	*Glu-74	*Asn-49		
*Thr-135	†Met-51		*Asp-62		
*Asp-139	Thr-54		‡Ala-63		
†His-169	Asp-55		‡Ile-64		
*Arg-217	*Asp-59		*Lys-65		
*Asp-392	*Arg-62		Ser-66		
	†Phe-63		*Lys-69		
	*Ser-71		*Glu-70		
	*Arg-73		*Ala-75		
	*Gln-74		Glu-130		
	*Asp-76		†Tyr-134		
	‡Arg-83		†Lys-146		
			*Gly-151		
			*Arg-154		
			*Glu-163		
			*Ile-208		
			†Glu-213		
			*Arg-216		
			*Asp-220		
			*Glu-223		
			*Glu-225		
			*Glu-227		
			His-233		
			‡Tyr-232		
			*Glu-235		
			*Tyr-236		
			Lys-240		
			‡Trp-241		
			†Glu-248		
			†Tyr-249		
			His-251		
			*Ile-293		
			†Arg-294		
			*Arg-299		

* Fully conserved residue.
† Conserved, except in a few species.
‡ Partially conserved.

Table S4. Suggested residue substitutions to probe binding sites 1/1'/2/2' in subunits Nqo4, Nqo6 and Nqo8.

Site	Substitution	Subunit	Reference
site 1	H38A/H38M/H38R	Nqo4	(3) but *cf.* also (6)
	H38Y/Y87H		
	Y87F/Y87W/Y87I/ Y87H/Y87S/Y87R	Nqo4	(7)
	D139N	Nqo4	(8)
	R217A	Nqo4	
site 1’	F63A	Nqo6	
site 2	W37A	Nqo6	
site 2'	W241A	Nqo8	
	Y249A	Nqo8	
	S66A	Nqo8	
	F28A	Nqo8	
	R62A	Nqo8	
	R36A	Nqo8	
	D62A	Nqo8	
	H233A	Nqo8	
	E225A	Nqo8	

Table S5. Organism list employed in multiple sequence alignments of Nqo8 (Fig. S8) and Nqo6 (Fig. S9).

Nqo8
Thermus thermophilus
Meiothermus ruber
Deinococcus misasensis
Thermogemmatispora carboxidivorans
Rhodococcus kunmingensis
Actinokineospora terrae
Escherichia coli
Shimwellia blattae
Franconibacter pulveris
Erwinia teleogrylli
Bos taurus
Neotragus batesi
Camelus dromedarius
Equus caballus
Sus scrofa
Martes zibellina
Felis chaus
Balaenoptera physalus
Ovis aries
Homo sapiens
Yarrowia lipolytica
Geotrichum candidum
Candida santjacobensis
Groenewaldozyma salmanticensis
Millerozyma farinosa
Wickerhamomyces canadensis
Sulfolobus solfataricus
Sulfolobales archaeon AZ1
Sulfolobus tokodaii
Pyrodictium delaneyi

Nqo6
Thermus thermophilus
Pyrinomonas methylaliphatogenes
Sulfobacillus acidophilus DSM 10332
Nitrospina gracilis
Streptomyces roseoverticillatus
Saccharothrix syringae
Bryobacter aggregatus
Escherichia coli
Erwinia iniecta
Rouxiella chamberiensis
Ewingella americana
Yersinia frederiksenii
Budvicia aquatica
Arsenophonus nasoniae
Bos taurus
Mus musculus
Larimichthys crocea
Xenopus tropicalis
Arabidopsis thaliana
Equus caballus
Sus scrofa
Ovis aries
Homo sapiens
Yarrowia lipolytica
Ceratocystis platani
Pestalotiopsis fici W106-1
Candida maltosa Xu316
Sphaerulina musiva SO2202
Paracoccidioides lutzii Pb01
Candidatus Heimdallarchaeota archaeon LC_2
Euryarchaeota archaeon RBG_13_61_15
Euryarchaeota archaeon RBG_16_68_12
Candidatus Caldiarchaeum subterraneum
Thermofilum adornatus

Table S6. Organism list employed in multiple sequence alignments of Nqo4 (see Fig. S10).

Nqo4
Thermus thermophilus
Meiothermus chliarophilus
Deinococcus marmoris
Limnochorda pilosa
Calditerrivibrio nitroreducens
Calderihabitans maritimus
Yuhushiella deserti
Sinorhizobium medicae
Gordonia paraffinivorans NBRC 108238
Pelosinus fermentans
Escherichia coli
Bos taurus
Camelus ferus
Lonchura striata domestica
Chrysemys picta bellii
Ovis aries
Homo sapiens
Yarrowia lipolytica CLIB122
Komagataella pastoris
Pichia kudriavzevii
Penicillium griseofulvum
Fonsecaea nubica
Tolypocladium paradoxum
Sulfolobus sp. A20
Archaeoglobus veneficus
Nitrosopumilus sp. Nsub

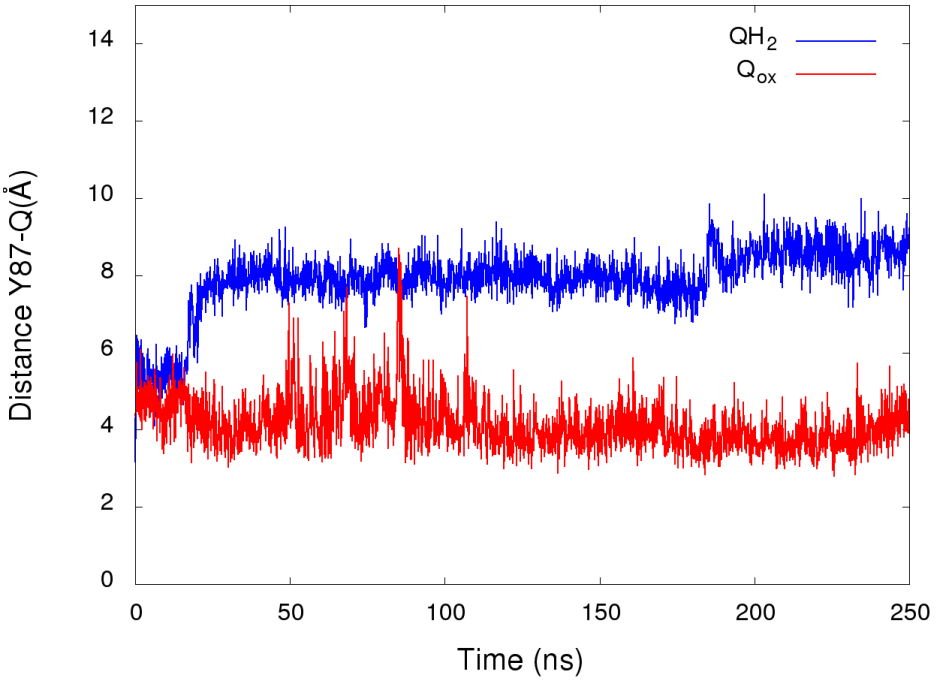

Figure S1. The distance of the Q headgroup from the active site Tyr-87_{Nqo4} for oxidized Q (in red) and QH_2 (in blue), obtained from 250 ns MD simulations of each state from simulation setup 2 (see Table S1).

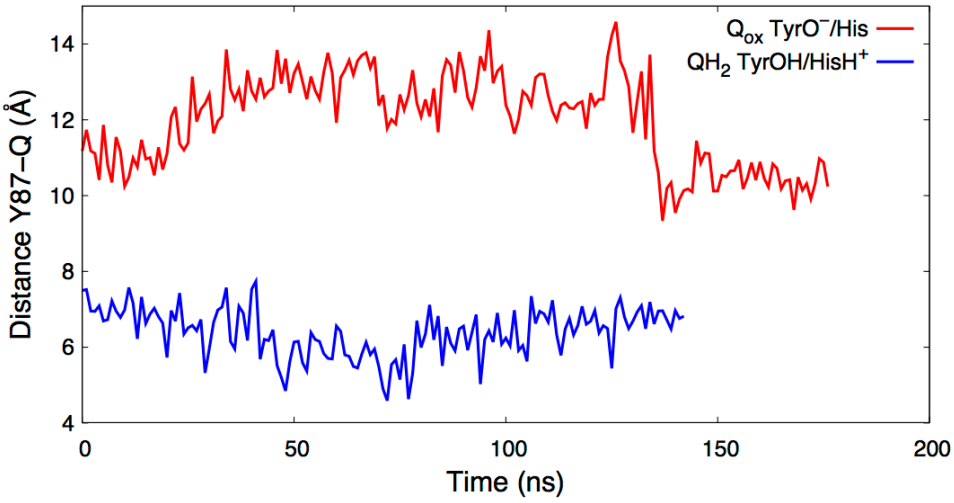

Figure S2. The distance between Tyr-87$_{Nqo4}$ and the Q headgroup. The Q is modeled as an oxidized Q (in red) and QH_2 (in blue) with active site structure corresponding to His/Asp$^-$/TyrO$^-$ and HisH$^+$/Asp$^-$/TyrOH states, respectively. The simulations were performed in simulation setup 1.

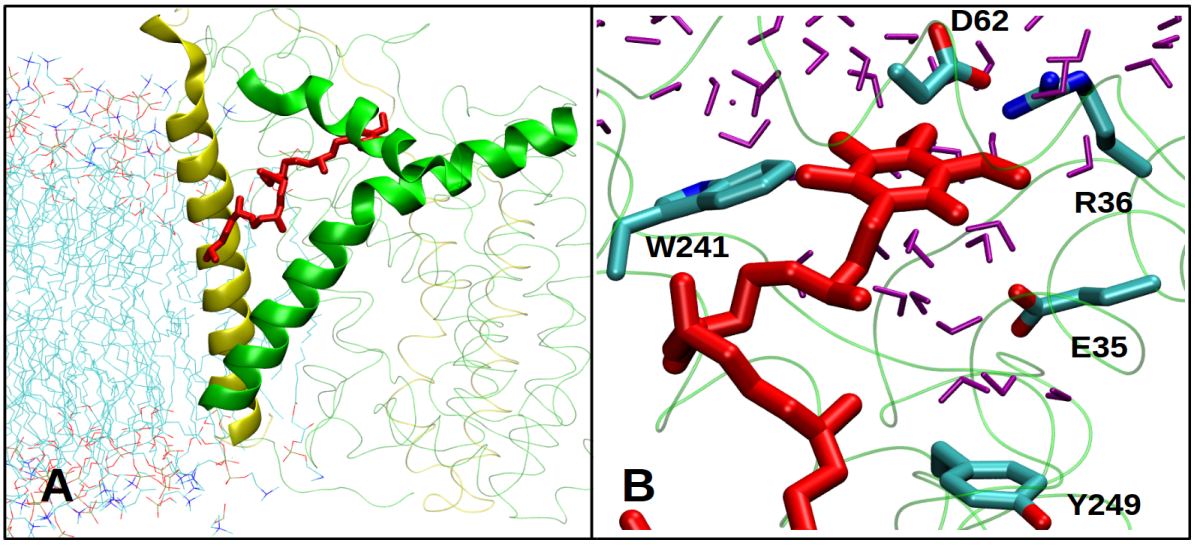

Figure S3. A) The quinone entry/exit site (2') is formed at an interface between three helices formed between subunits Nqo8 (in green) and Nqo7 (in yellow). B) Close-up of the quinone modeled near the exit site.

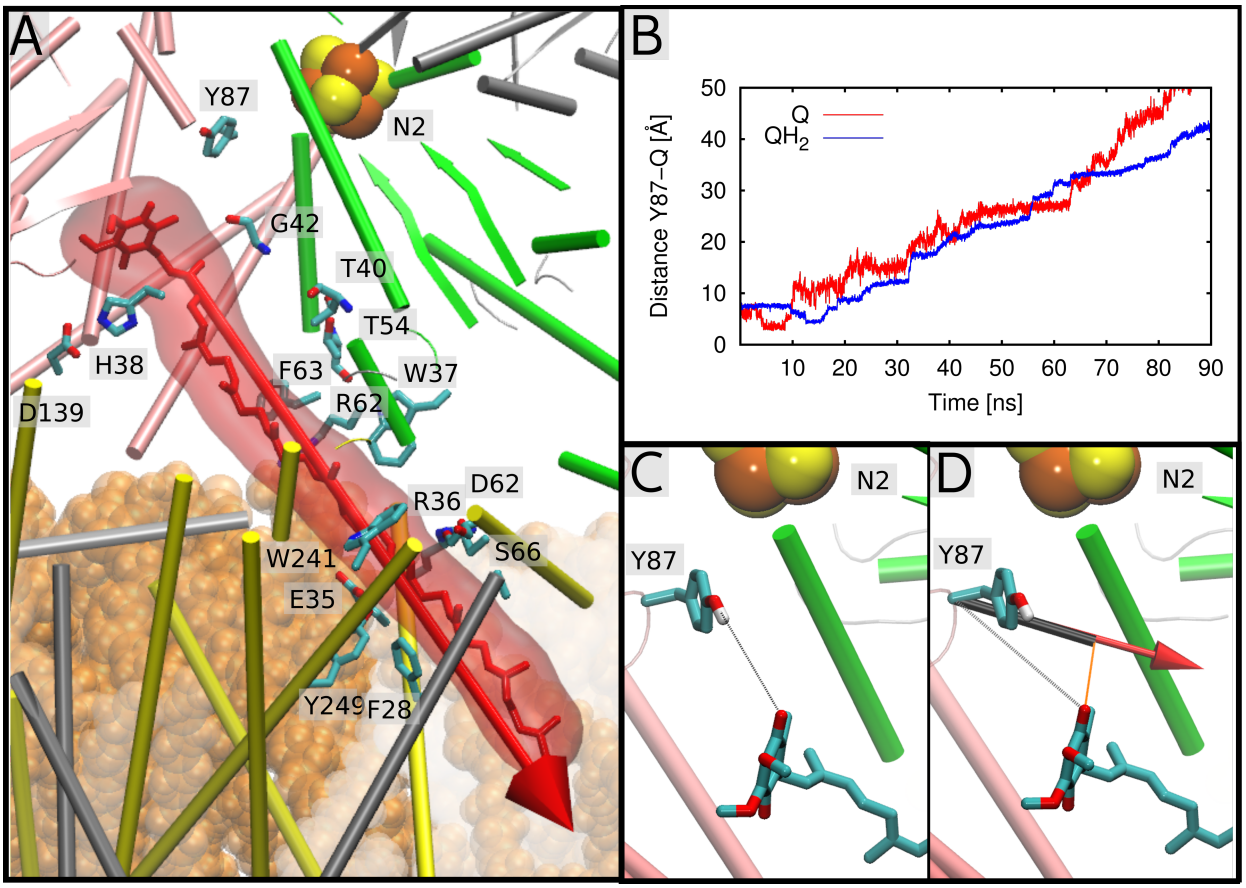

Figure S4. SMD simulations of Q_{ox} and QH_2. A) Oxidized Q (in red) bound in the primary binding site 1. The force acting on the complete Q_{ox}/QH_2 molecule during the SMD simulations is shown with a red arrow. B) The SMD pulling distance as a function of simulation time, showing the distance between hydroxyl oxygen of Tyr-87_{Nqo4} and the carbonyl oxygen (closest to Tyr-87_{Nqo4}) of the Q_{ox}/QH_2 headgroup. In the SMD simulations, the Q_{ox}/QH_2 molecule is pulled towards the membrane exit of its binding cavity. Illustration of the reaction coordinates: C) the minimum distance between Tyr-87(OH) and the carbonyl oxygen of the Q headgroup, D) the projected minimum distance (in black) between Tyr-87_{Nqo4}(Cα) and the carbonyl oxygen of the Q headgroup on the SMD pulling vector (in red).

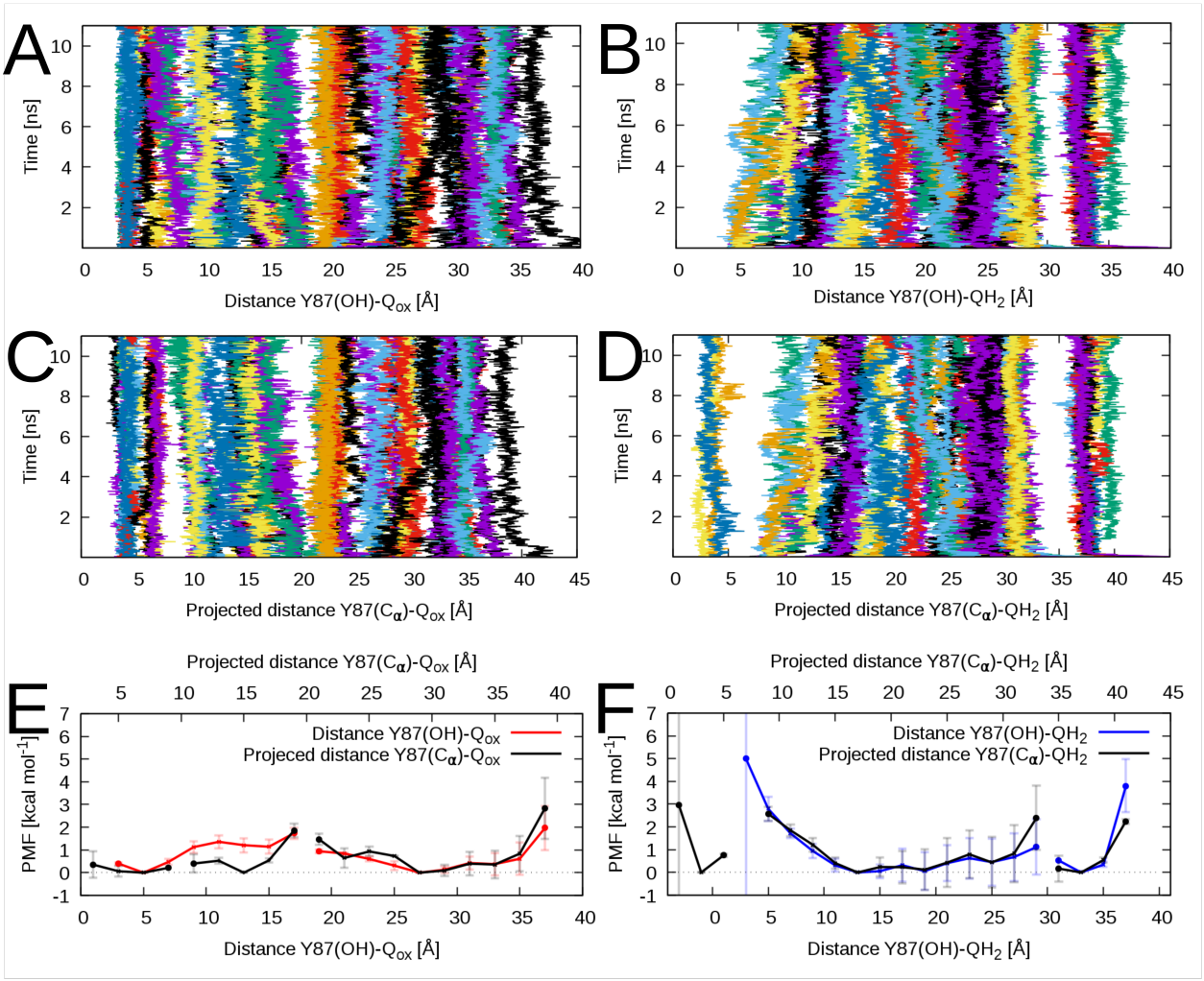

Figure S5. Overlap of reaction coordinates in A) and C) 65 x 11 ns MD simulations that were employed for constructing diffusion model for Q, and B) and D) in 54 x 11 ns and 57 x 11 ns MD simulations of QH_2. Panels A and B show sampling of the minimum distance Tyr-87_{Nqo4}(OH)-Q headgroup reaction coordinate. Panels C and D show sampling of the projected minimum distance Tyr-87_{Nqo4}(Cα)-Q headgroup reaction coordinate (see Method, Fig. S4). E) PMF profiles for the oxidized quinone using the projected Tyr-87_{Nqo4}(Cα)-Q_{ox} headgroup distance (black) and Tyr-87_{Nqo4}(OH)-Q_{ox} headgroup (red) distance as reaction coordinate. F) PMF profiles of reduced quinol using the projected Tyr-87_{Nqo4}(Cα)-QH_2 headgroup distance (black) and distance Tyr-87_{Nqo4}(OH)- QH_2 headgroup (blue) as reaction coordinate. The simulations are based on setup 2. Error bars in the PMF indicate standard errors of the mean, which were estimated by block averaging (see Methods).

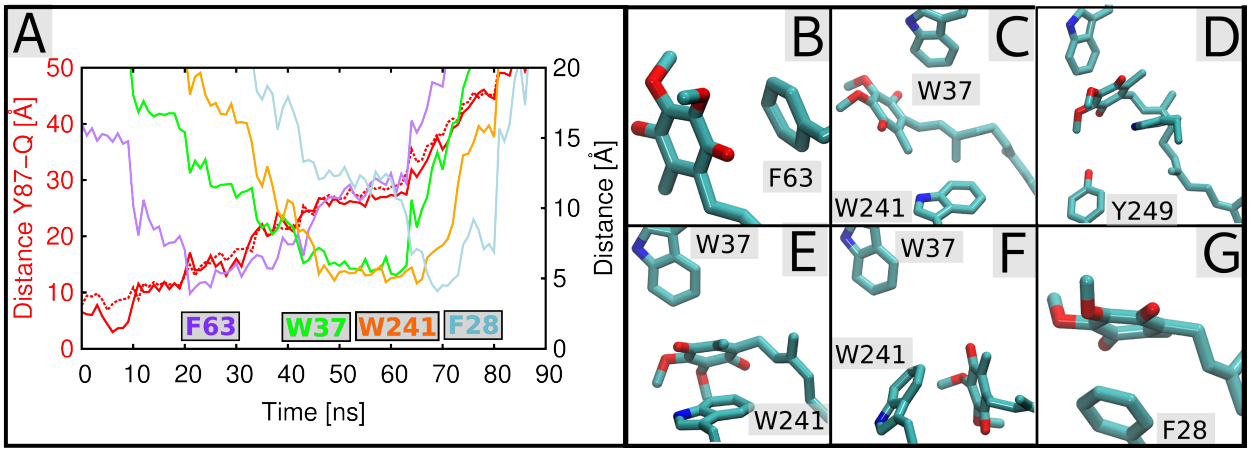

Figure S6. SMD simulations of oxidized Q. A) Pulling distance as a function of the SMD simulation time between the center of mass of the Q headgroup and the center of mass of interacting protein residues. The figure highlights interactions with residues Phe-63_{Nqo6} (in purple), Trp-37_{Nqo6} (in green), Trp-241_{Nqo8} (in orange), and Phe-28_{Nqo8} (in light blue). The distance is measured between the Q headgroup (carbonyl oxygen O2, in red, and O5, in dashed red) and the hydroxyl oxygen of Tyr-87_{Nqo4}. B-G) Snapshots from the SMD simulation when the Q headgroup is stabilized by specific interactions with the selected amino acids. The snapshots are numbered in time sequence of the SMD trajectory. Snapshot of Q interacting with (B) Phe-63_{Nqo6} at 24 ns, (C) with Trp-37_{Nqo6} at 44 ns, (D) with Tyr-249_{Nqo8} at 56 ns, (E) with Trp-241_{Nqo8} at 63 ns, which comprises the second binding site (see main text). (F) Snapshot of the Q headgroup interacting with Tyr-241_{Nqo8} at 64 ns after passing the second binding site, and (G) with Q in site 2', forming interactions with Phe-28_{Nqo8} at 69 ns.

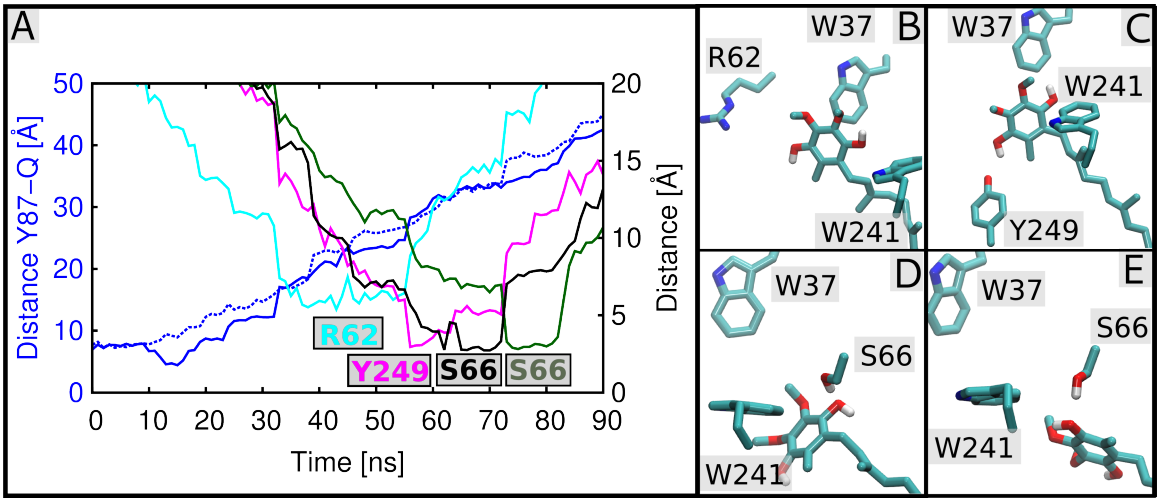

Figure S7. SMD simulations of reduced QH_2. A) Pulling distance as a function of the SMD simulation time between the Q headgroup (carbonyl oxygen O2, in blue, and O5, in dashed blue) and the hydroxyl oxygen of Tyr-87_{Nqo4}. The figure highlights interactions with residues Arg-62_{Nqo6} (in cyan), Tyr-249_{Nqo6} (in magenta), and Ser-66_{Nqo8} (black/green). The distance is measured between the Q headgroup (carbonyl oxygen O2, in blue, and O5, in dashed blue) and the hydroxyl oxygen of Tyr-87_{Nqo4}. B-E) Snapshots from the SMD simulation when the QH_2 headgroup is stabilized by specific interactions with the selected amino acids. The snapshots are numbered in time sequence of the SMD trajectory. Snapshot of QH_2 headgroup interacting with B) Arg-62_{Nqo6} at 55 ns, C) Tyr-249_{Nqo8} at 56 ns, D) Ser-66_{Nqo8} at 66 ns, and E) at 77 ns.

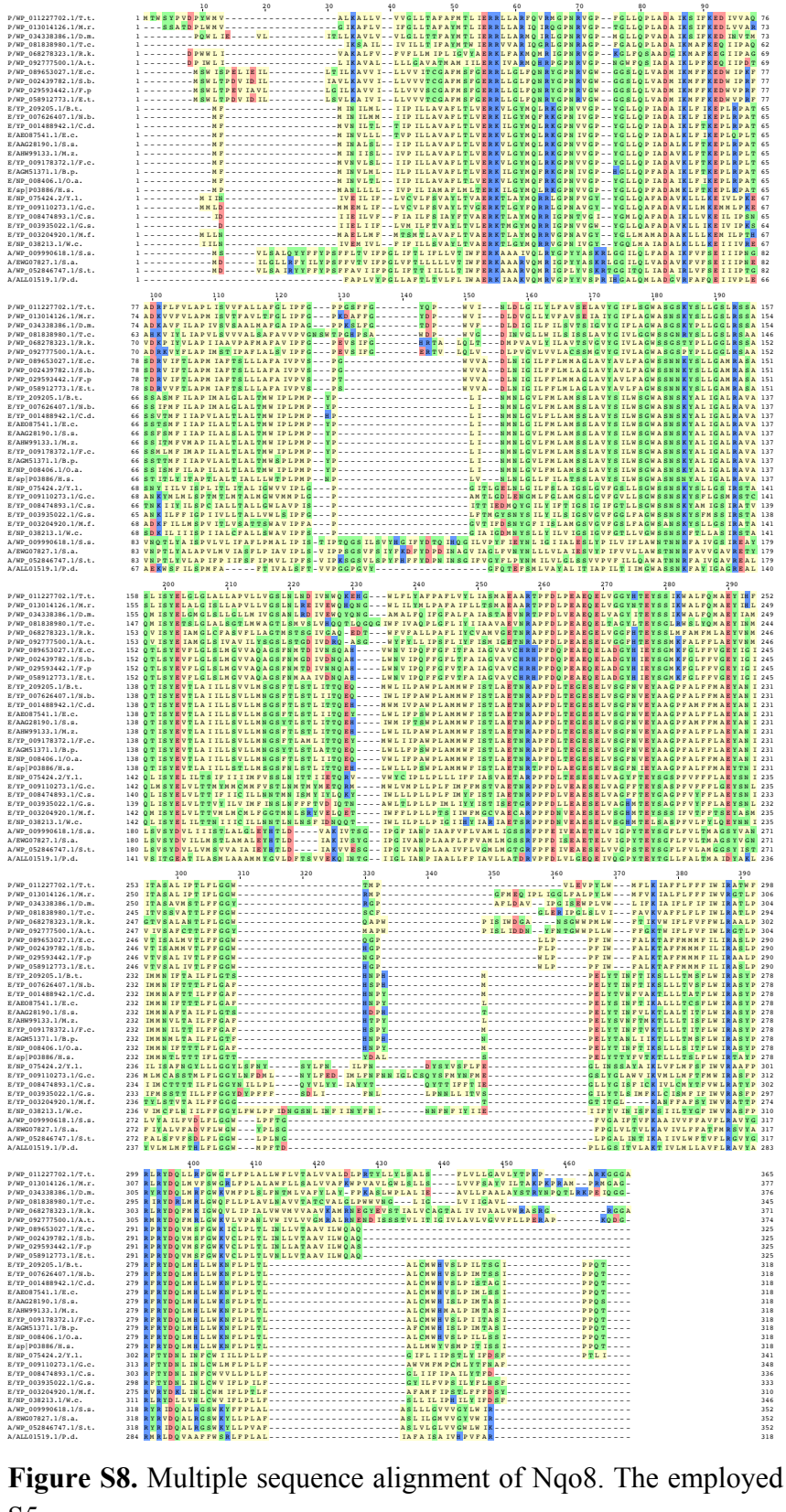

Figure S8. Multiple sequence alignment of Nqo8. The employed organisms are shown in Table S5.

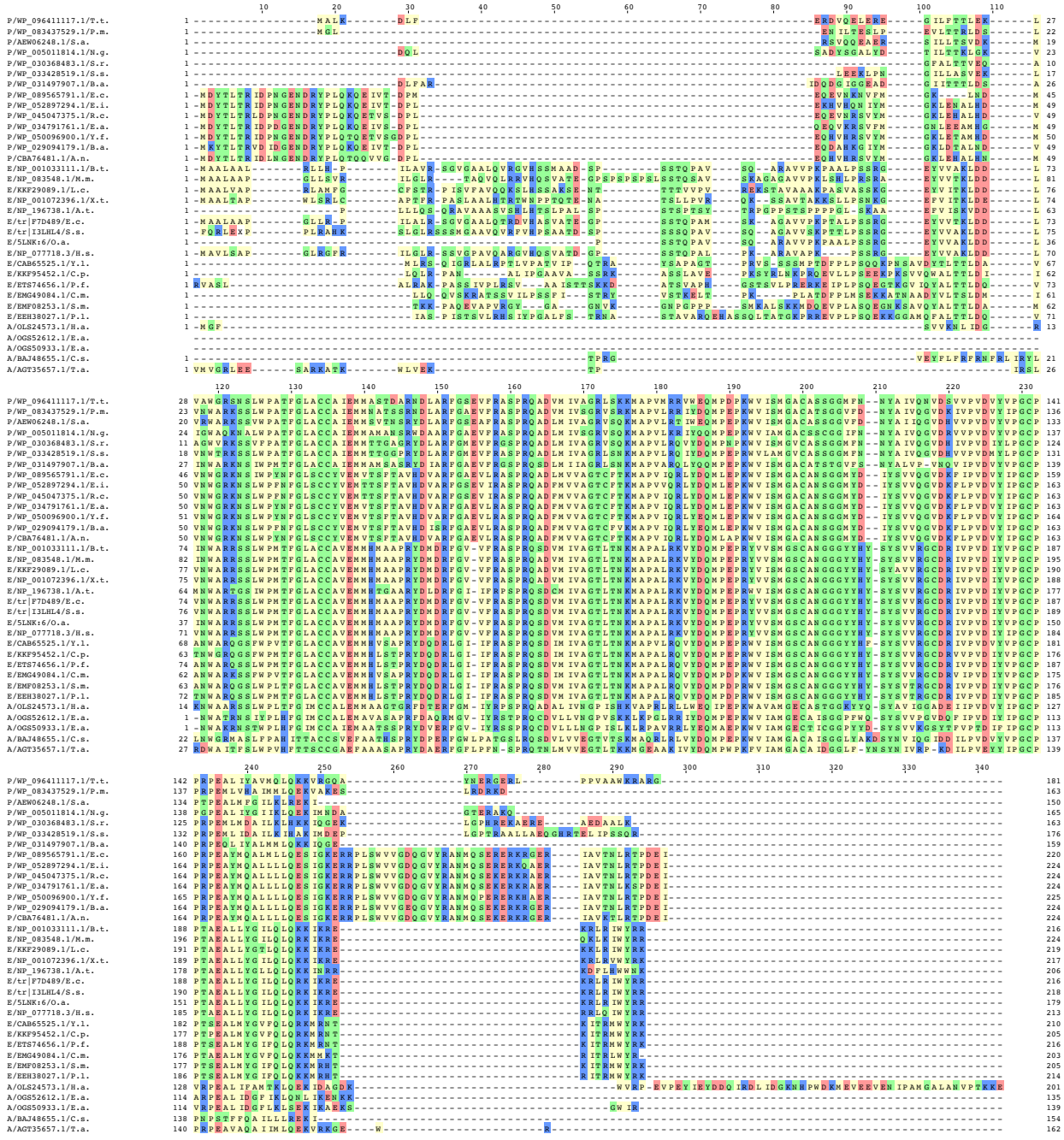

Figure S9. Multiple sequence alignment of Nqo6. The employed organisms are shown in Table S5.

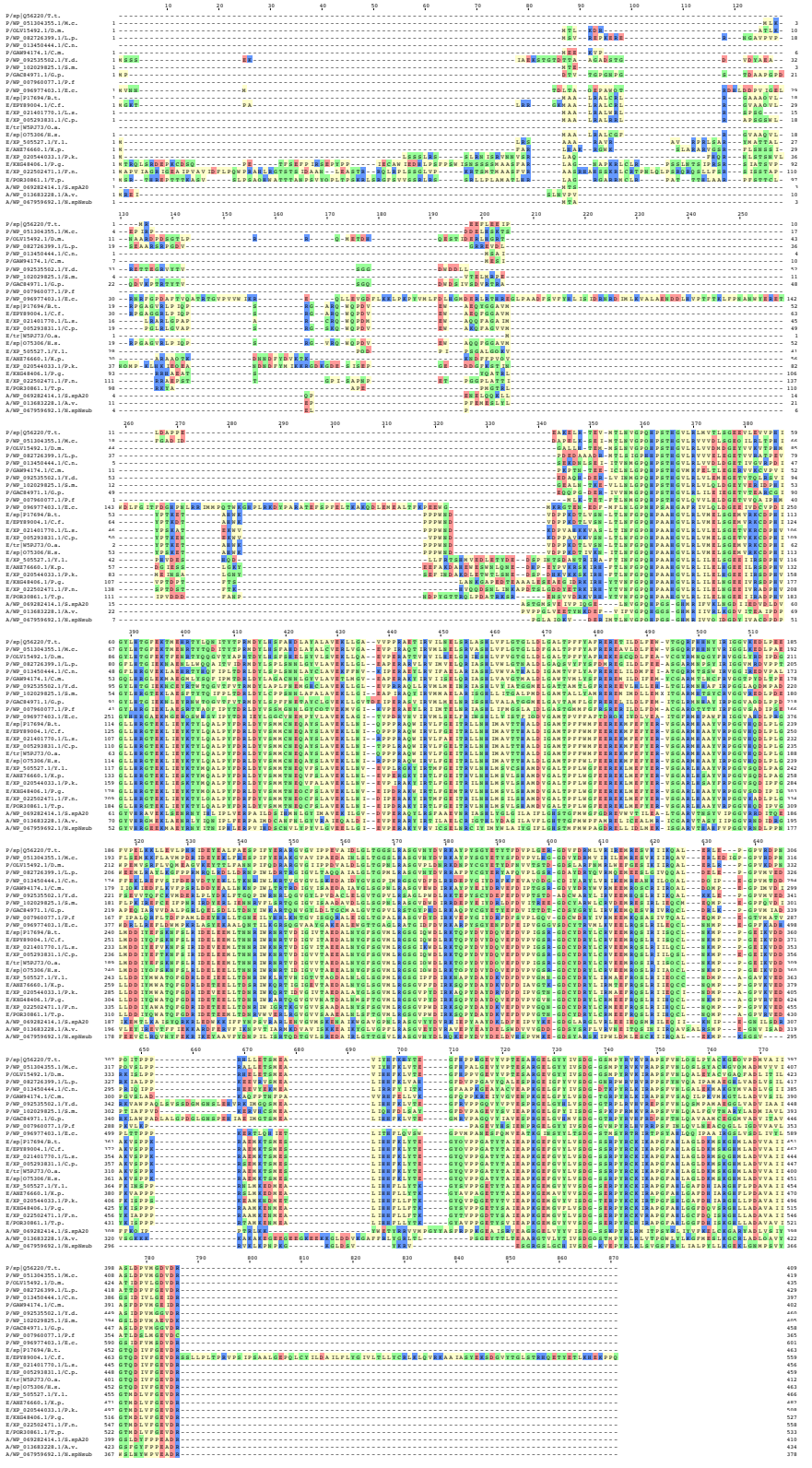

Figure S10. Multiple sequence alignment of Nqo4. The employed organisms are shown in Table S6.

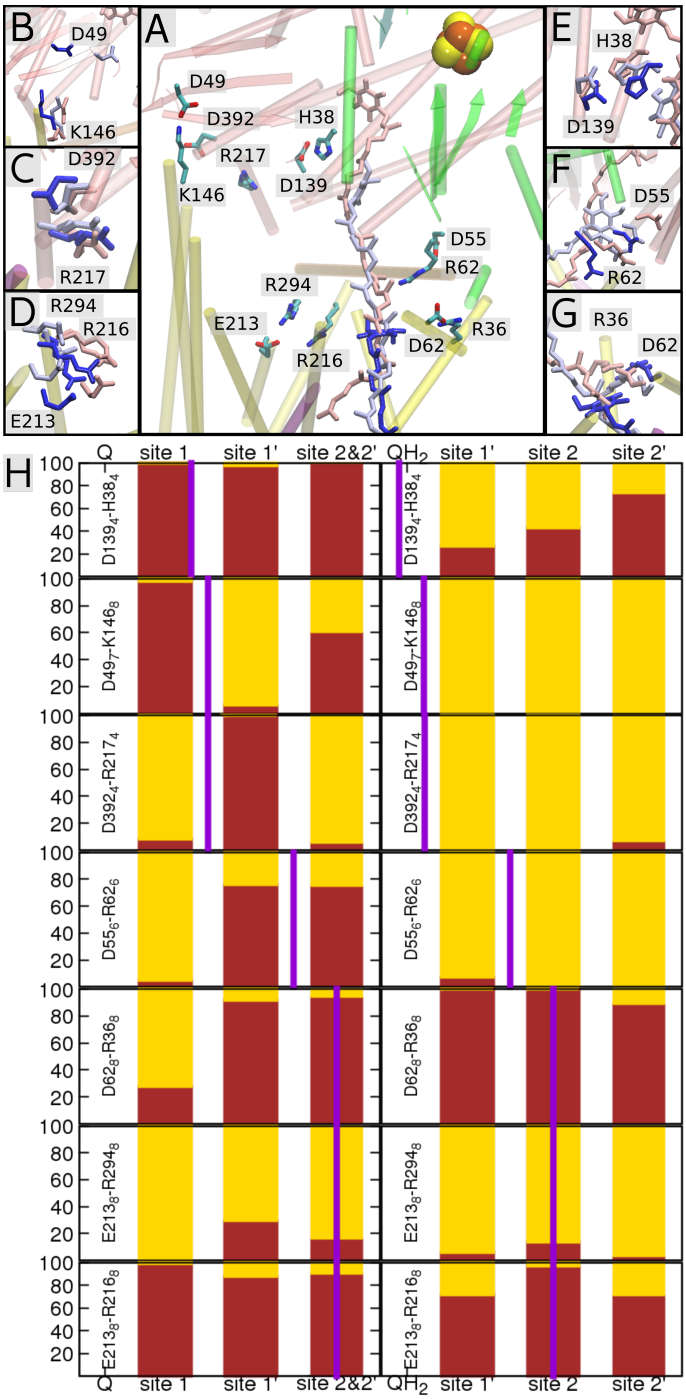

Figure S11. Analysis of ion-pair conformations in subunits Nqo4 and Nqo6-Nqo10 during equilibrium MD simulations of Q_{ox} and QH_2 at different positions of the Q-channel (A). The figure shows ion-pairs between B) Asp-49$_{Nqo7}$/Lys-146$_{Nqo8}$, C) Asp-392$_{Nqo4}$/Arg-217$_{Nqo4}$, D) Glu-213$_{Nqo8}$/Arg-294$_{Nqo8}$ and Glu-213$_{Nqo8}$/Arg-216$_{Nqo8}$, E) Asp-139$_{Nqo4}$/His-38$_{Nqo4}$, F) Asp-55$_{Nqo6}$/Arg-62$_{Nqo6}$, and G) Asp-62$_{Nqo8}$/Arg-36$_{Nqo8}$. H) Analysis of open (in yellow) and closed (in red) ion-pairs when Q_{ox} and QH_2 residues in PMF site 1/1', and site 2, site 2' (see main text Figure 4, and main text). A distance criteria of 5 Å was employed for the opening threshold of the ion-pairs. The purple lines indicate that the Q resides is the vicinity of the marked ion-pair.

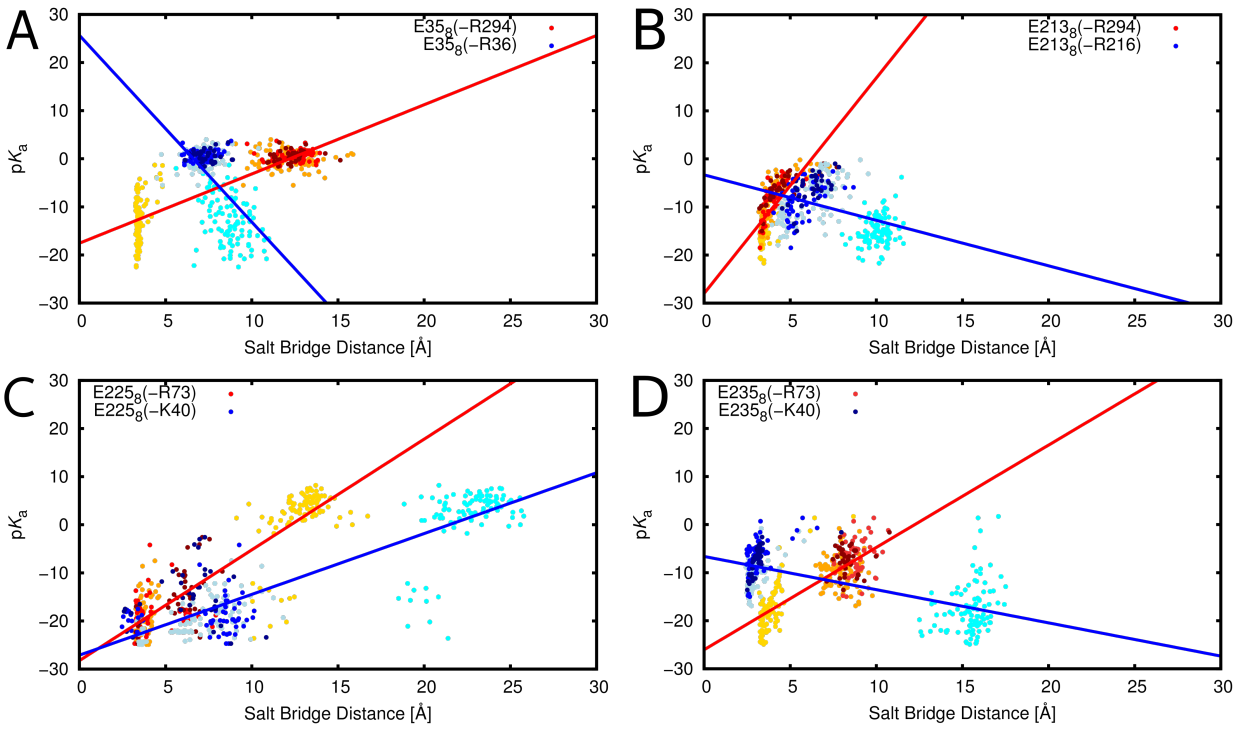

Figure S12. Correlation of pK_a for Glu-35$_{Nqo8}$ (A), Glu-213$_{Nqo8}$ (B), and Glu-225$_{Nqo8}$ (C), and Glu-235$_{Nqo8}$ (D) with ion-pair distances of Glu-35$_{Nqo8}$/Arg-36$_{Nqo8}$ (A), Glu-35$_{Nqo8}$/Arg-294$_{Nqo8}$ (A), Glu-213$_{Nqo8}$/Arg-294$_{Nqo8}$ (B), Glu-213$_{Nqo8}$/Arg-216$_{Nqo8}$ (B), Glu-225$_{Nqo8}$/Lys-40$_{Nqo7}$ (C), Glu-225$_{Nqo8}$/Arg-73$_{Nqo6}$ (C), Glu-235$_{Nqo8}$/Arg-73$_{Nqo6}$ (D), and Glu-235$_{Nqo8}$/Lys-40$_{Nqo7}$ (D). The simulations were based on setup 2. Depending on Tyr-87$_{Nqo4}$ - Q_{ox} headgroup distance of each frame a pK_a and ion pair distance is measured, which determines the color of the points. When Q_{ox} is in binding site 1 (Tyr-87$_{Nqo4}$-Q_{ox} distance < 6 Å) the pK_a values as function of the ion pair distance is shown in yellow and cyan points, when Q_{ox} is in binding site 1' (Tyr-87$_{Nqo4}$-Q_{ox} distance > 6 Å and < 20 Å) the pK_a values as function of the ion pair distance is shown in orange and light-blue points, Q_{ox} bound in site 2 (Tyr-87$_{Nqo4}$-Q_{ox} distance > 20 Å and < 27 Å) the pK_a values as function of the ion pair distance is shown in red and blue points, Q_{ox} is in binding site 2' (Tyr-87$_{Nqo4}$-Q_{ox} distance > 27 Å) the pK_a values as function of the ion pair distance is shown in dark-red and dark-blue points. Linear fit of each ion pair (red and blue lines).

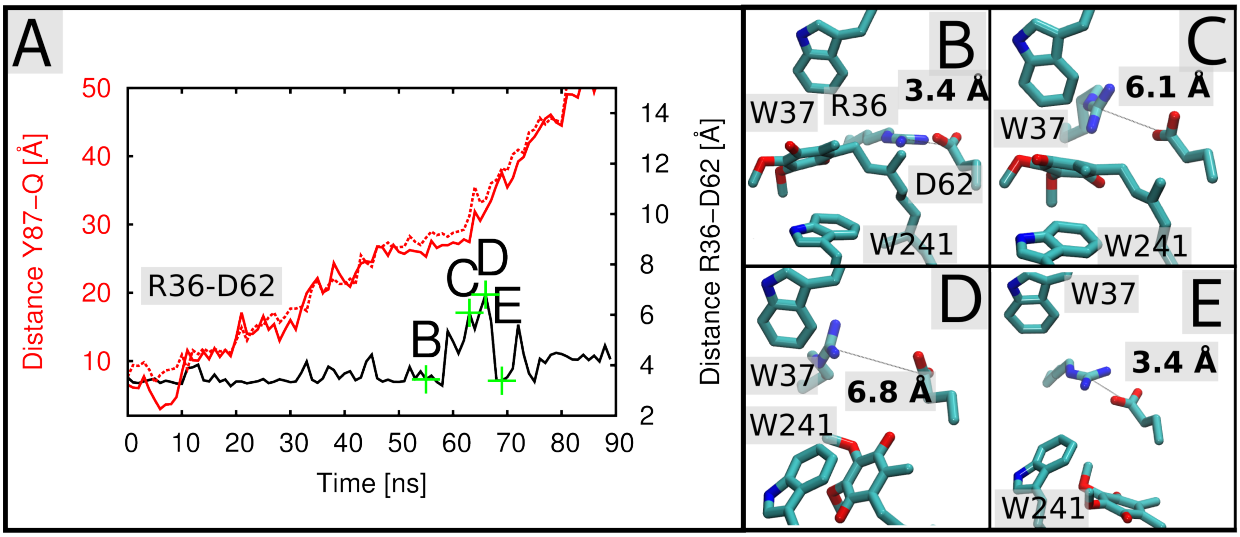

Figure S13. A) Correlation between the Tyr-87$_{Nqo4}$-Q distance and the opening of the conserved ion-pair Arg-36/Asp-62$_{Nqo8}$ obtained from an SMD simulation. Experiments suggest that the Arg-36/Asp-62 ion-pair is functionally important in complex I (see Table S3). B-E) Selected structural snapshots along the SMD trajectory are indicated with green crosses and the corresponding labels in panel A. B-E) Snapshots of Q_{ox} and the Arg-36/Asp-62$_{Nqo8}$ ion-pair along the SMD trajectory. (B) Q in the second binding site (site 2), forming an interaction with Trp-241$_{Nqo8}$ at 55 ns, and (C) at 63 ns, upon dissociation of the Arg-36/Asp-62$_{Nqo8}$ ion-pair. D) Q_{ox} interacting with Trp-241$_{Nqo8}$ at 66 ns. The Arg-36/Asp-62$_{Nqo8}$ ion-pair is re-established after Q passes this binding site.

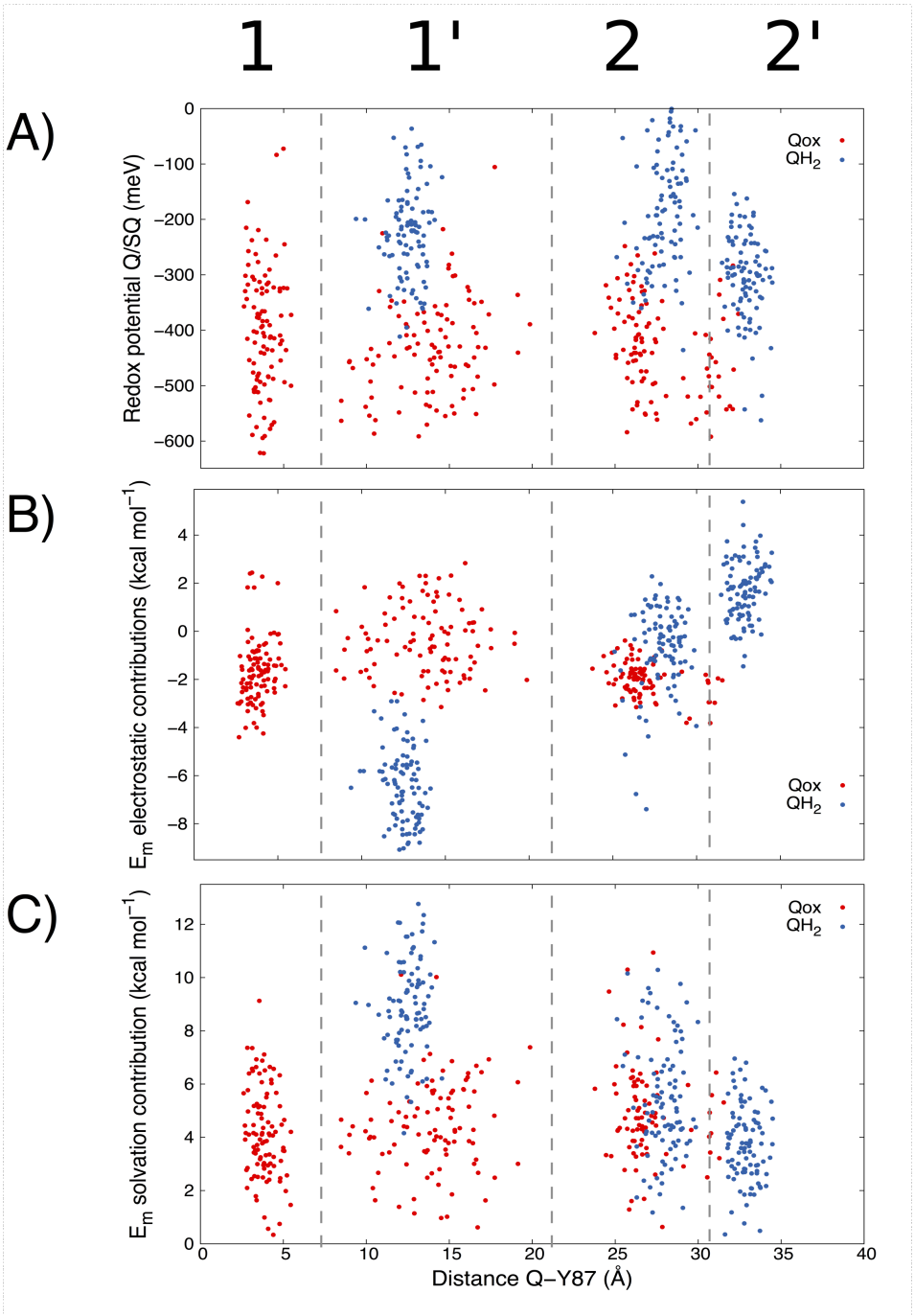

Figure S14. A) Redox potential, E_m, calculated with Poisson-Boltzmann electrostatics of the Q_{ox}/SQ pair along the binding sites of Q_{ox} and QH_2 cavities. The fluctuations of the calculations are large (*ca*. 200 mV), but qualitatively the binding site environment for QH_2 is favored for electron transfer in comparison with Q_{ox}. B) Electrostatic contribution and C) solvation contribution to the E_m values obtained in A.

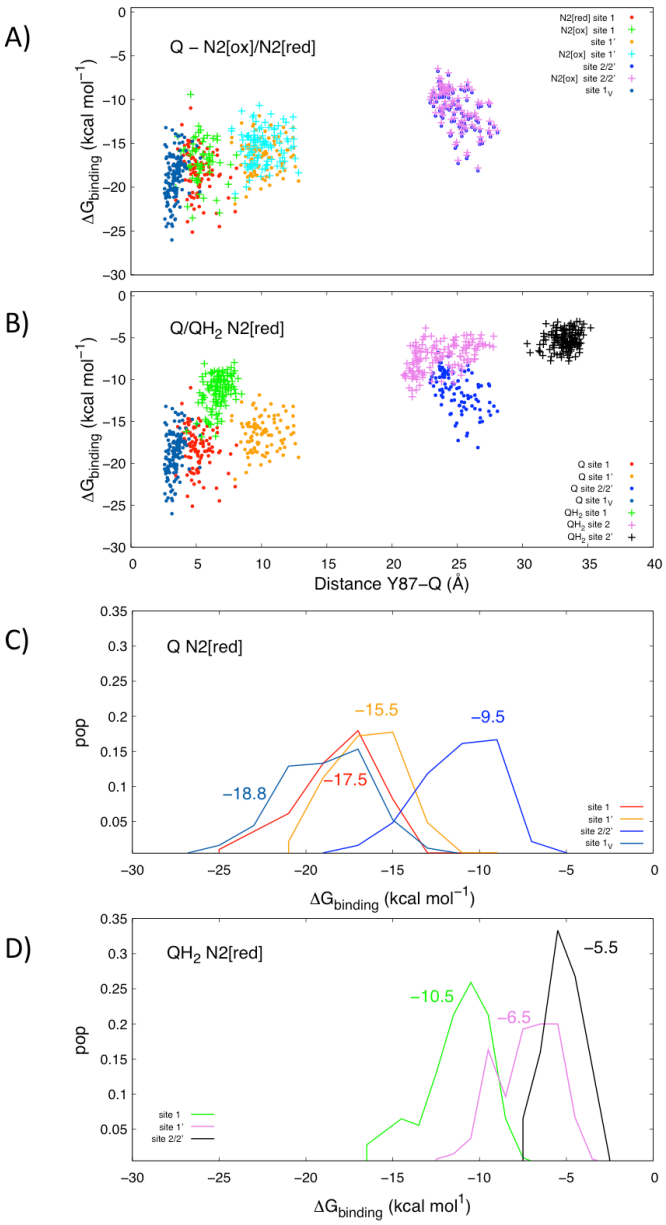

Figure S15. Binding energies for Q_{ox} and QH_2 along the quinone cavity binding sites 1, 1', and 2/2' from setup 2. Data from previous simulations (8) are marked as "site 1_v". A) Comparison of binding energies when the iron-sulfur center N2 is modelled in the oxidized (N2[ox]) or reduced (N2[red]) state, respectively. B) Comparison of binding energies for Q_{ox} and QH_2 with reduced N2 iron-sulfur center. C) Histogram of binding energies for Q_{ox} and D) for QH_2. Arithmetic averages of binding energies are given on top of each histogram.

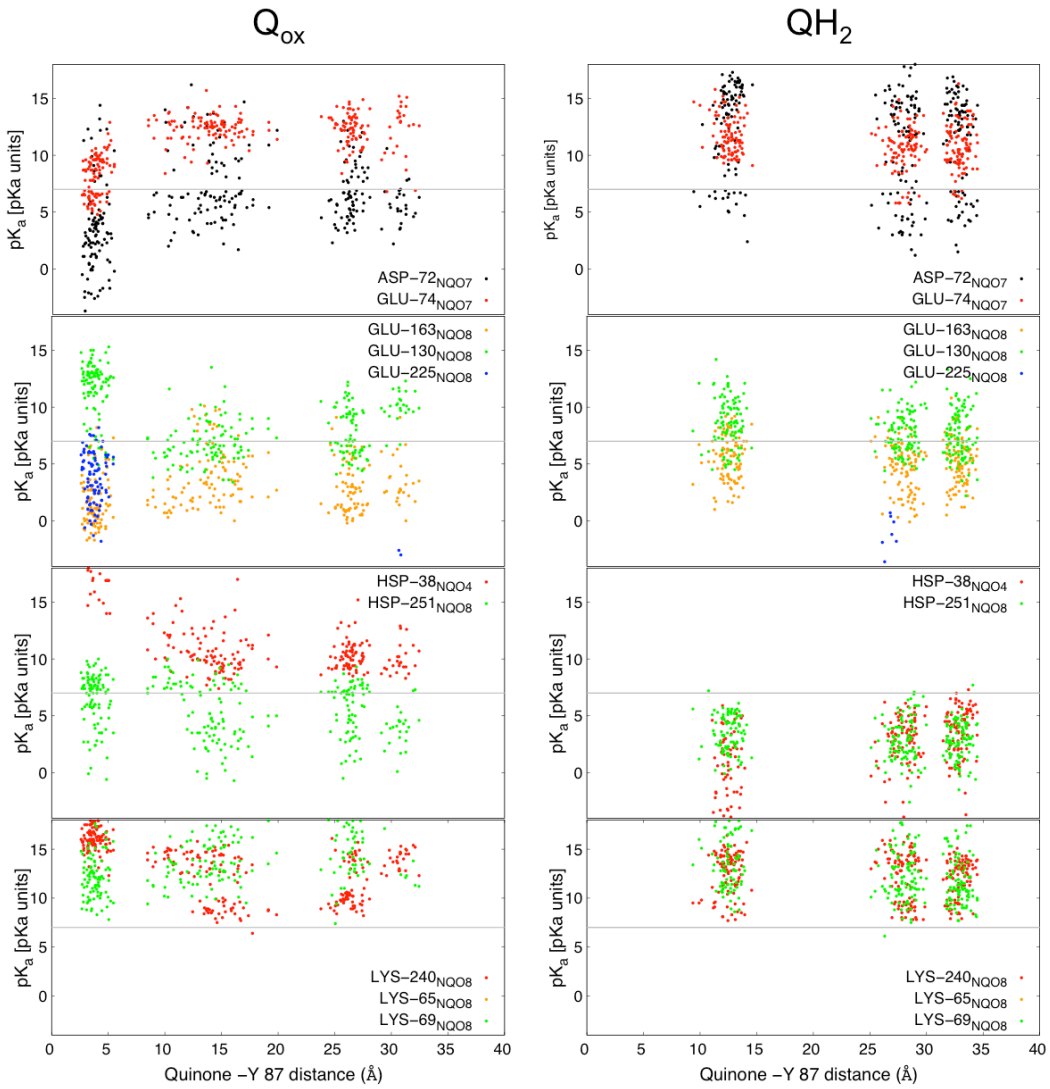

Figure S16. Poisson-Boltzmann (PB) electrostatic calculations and protonation probabilities of titratable amino acids near the Q-cavity in selected frames along the reaction coordinate for Q_{ox} and QH_2 simulations in setup 2, pK_a=7 is indicated by a gray line. Titratable amino acids whose protonation state does not deviate from the standard protonation state are not shown in the plots (*e.g.* Tyr-87$_{Nqo4}$, Tyr-249$_{Nqo8}$ are predicted protonated, whereas Glu-35$_{Nqo8}$, Glu-223$_{Nqo8}$, Glu-248$_{Nqo8}$, and Glu-235$_{Nqo8}$ are predicted deprotonated in the PB calculations).

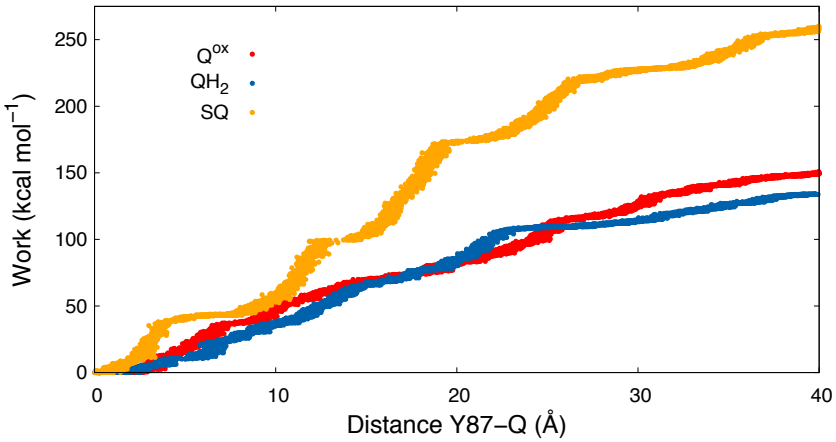

Figure S17. Calculated work (in kcal mol^{-1}) as a function of the distance Q and Tyr-87_{Nqo4} (OH), calculated from SMD simulations of Q_{ox}, SQ, and QH_2. Simulations are based on setup 1.

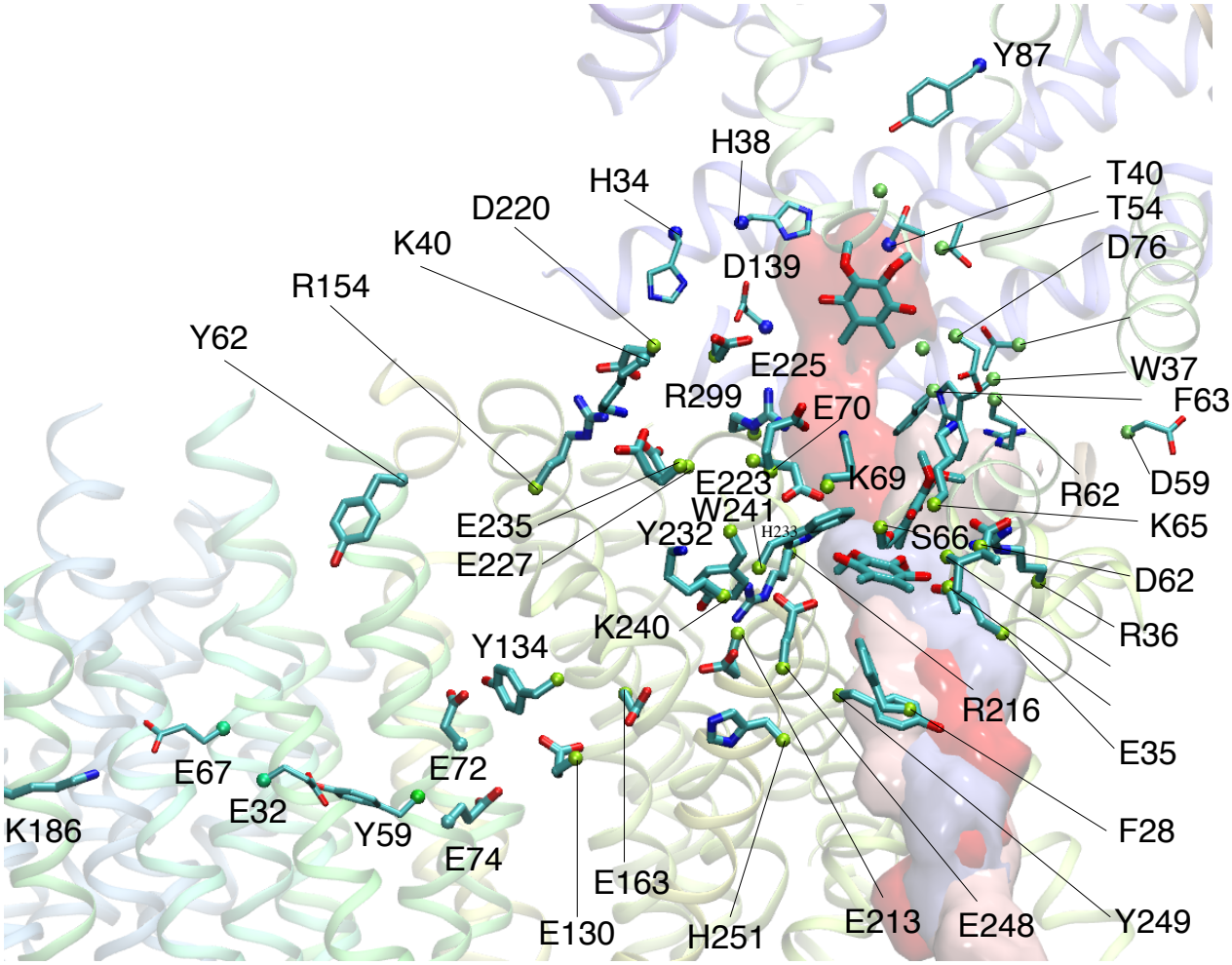

Figure S18. Quinone binding cavity indicating the Q binding sites with binding site 1 (in red), site 1' (in pink), and site 2/2', (in blue) along with the amino acids that form interactions with Q along the cavity. The Cα atoms are colored according to the subunit, with Nqo6 (in blue), Nqo6 (in light green), Nqo8 (in dark green), Nqo7 (in yellow), and Nqo11 (in green).

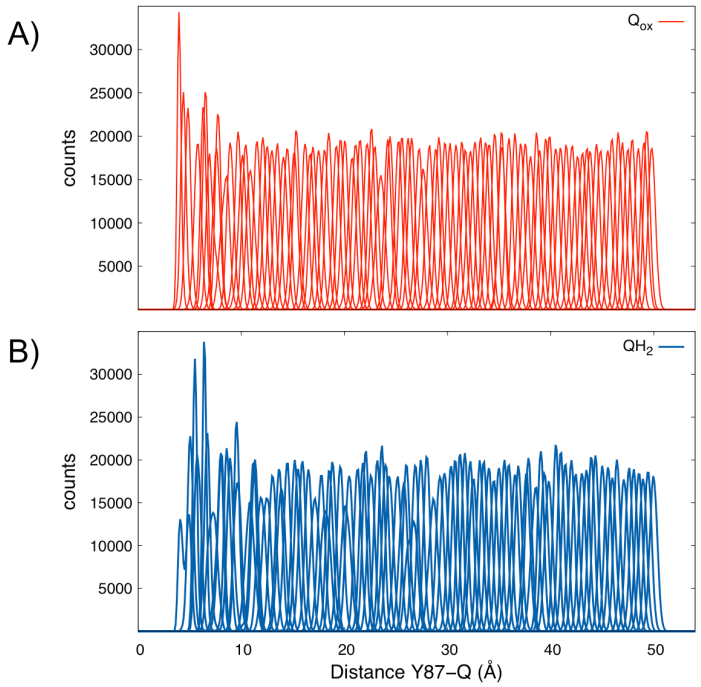

Figure S19. Overlap of the sampled Tyr-87_{Nqo4} - Q distance in the umbrella sampling simulations (of Q_{ox} and QH_2). Simulations are based on setup 3.

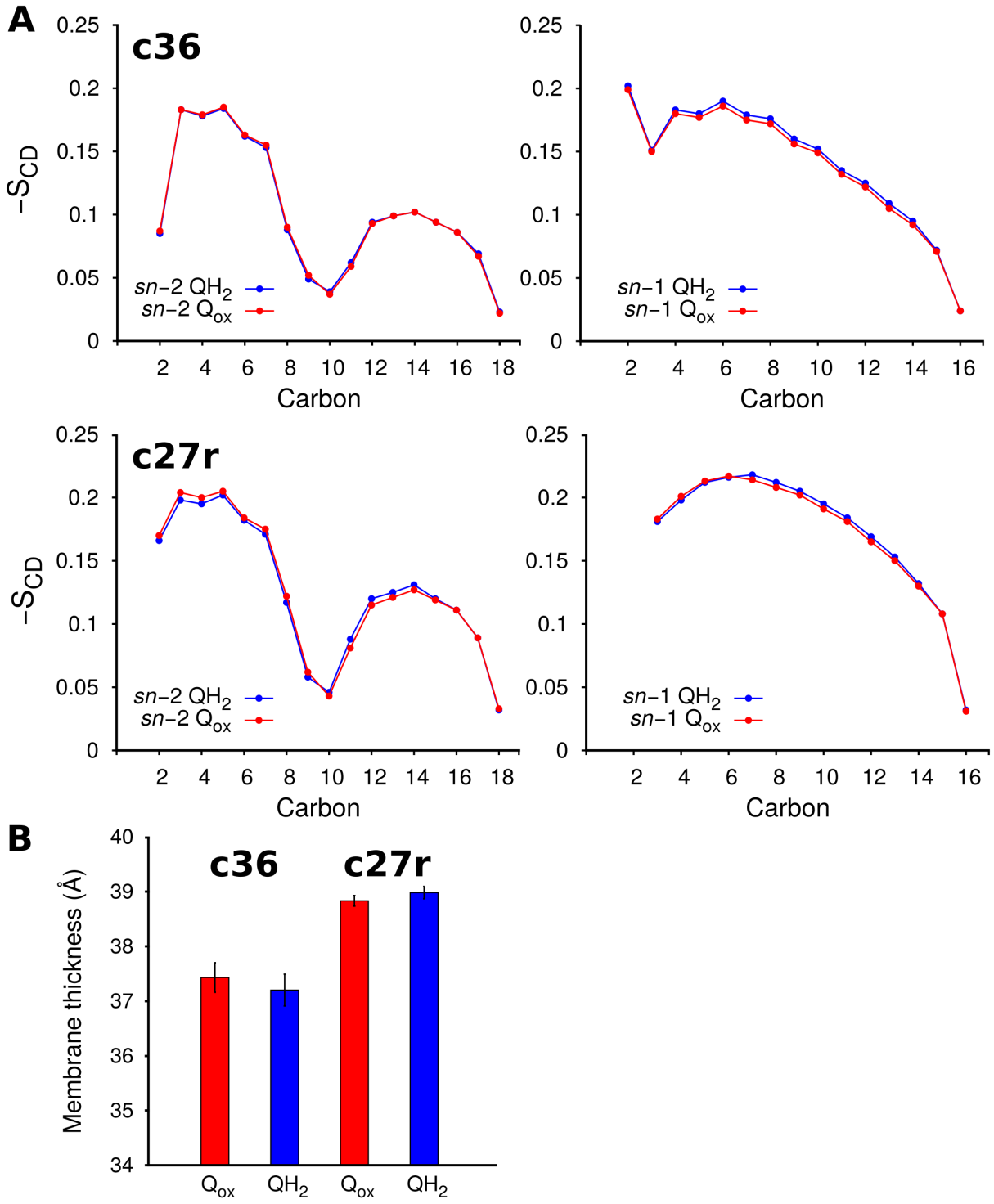

Figure S20. Equilibration of lipid membrane during the MD simulations for Q_{ox} and QH_2 obtained with CHARMM27 (c27r) and CHARMM36 (c36) force fields. A) acyl chain (sn-1 and sn2) deuterium order parameter (S_{CD}) of the POPC lipid chains and B) membrane thickness equilibrate to literature values (9, 10) within the initial 100 ns of the MD simulations.

References

1. Baradaran R, Berrisford JM, Minhas GS, Sazanov LA (2013) Crystal structure of the entire respiratory complex I. *Nature* 494:443-448.
2. Garofano A, Zwicker K, Kerscher S, Okun P, Brandt U (2003) Two aspartic acid residues in the PSST-Homologous NUKM subunit of Complex I from Yarrowia lipolytica are essential for catalytic activity. *J Biol Chem* 278:42435-42440.
3. Grgic L, Zwicker K, Kashani-Poor N, Kerscher S, Brandt U (2004) Functional significance of conserved histidines and arginines in the 49-kDa subunit of mitochondrial complex I. *J Biol Chem* 279:21193.
4. Tocilescu MA, Fendel U, Zwicker K, Kerscher S, Brandt U (2007) Exploring the Ubiquinone Binding Cavity of Respiratory Complex I. *J Biol Chem* 282:29514-29520.
5. Sinha PK, Torres-Bacete J, Nakamaru-Ogiso E, Castro-Guerrero N, Matsuno-Yagi A, Yagi T (2009) Critical Roles of Subunit NuoH (ND1) in the Assembly of Peripheral Subunits with the Membrane Domain of Escherichia coli NDH-1. *J Biol Chem* 284:9814-9823.
6. Sinha P.K., Castro-Guerrero N., Patki G., Sato M., Torres-Bacete J., Sinha S., Miyoshi H., Matsuno-Yagi A., Yagi T. (2015) Conserved amino acid residues of the NuoD segment important for structure and function of Escherichia coli NDH-1 (complex I) *Biochemistry* 54:753–764.
7. Tocilescu MA, Fendel U, Zwicker K, Dröse S, Kerscher S, Brandt U (2010) The role of a conserved tyrosine in the 49-kDa subunit of complex I for ubiquinone binding and reduction. *Biochim Biophys Acta* 1797:625–632.
8. Sharma V, Belevich G, Gamiz-Hernandez AP, Rog T, Vattulainen I, Verkhovskaya ML, Wikström M, Hummer G, Kaila VRI (2015) Redox-Induced Activation of the Proton Pump in the Respiratory Complex I. *Proc Natl Acad Sci USA* 112:11571-11576.
9. Kučerka N, Nieh M-P, Katsaras J (2011) Fluid phase lipid areas and bilayer thicknesses of commonly used phosphatidylcholines as a function of temperature. *Biochim Biophys Acta - Biomembranes* 1808:2761–2771.
10. Klauda JB, Venable RM, Freites JA, O'Connor JW, Tobias DJ, Mondragon-Ramirez C, Vorobyov I, MacKerell AD, Pastor RW (2010) Update of the CHARMM All-Atom Additive Force Field for Lipids: Validation on Six Lipid Types. *J Phys Chem B* 114:7830-7843.